AIAA JOURNAL
Vol. 50, No. 12, December 2012

Technical Notes

Flapping Flight: High Thrust and Propulsive Efficiency due to Forward Gliding Oscillations

Stephan E. Bansmer* and Rolf Radespiel†
Technische Universität Braunschweig, 38106 Braunschweig, Germany

DOI: 10.2514/1.J051749

I. Introduction

THE flapping flight mechanism can provide revolutionary operation capabilities for tomorrow's micro air vehicles (MAV) [1]. The unsteady aerodynamics of the flapping flight is vastly different from traditional fixed-wing flyers and allows for high maneuverability in cluttered environments [2]. To provide this maneuverability, high rates of thrust and propulsive efficiency beyond normal cruise flight conditions are necessary. Observations of flying birds in nature [3] revealed that birds are not only using the classic combined pitch/plunge motion for flapping flight but also incorporate an additional gliding motion of their wings in the direction of the free-stream velocity U_∞. The present note demonstrates that these gliding motions increase significantly both thrust and efficiency of flapping flight. For this purpose, unsteady Reynolds-averaged Navier–Stokes (URANS) computations are used to estimate the flow around a flapping, birdlike airfoil SG04 [4] at a Reynolds number of 10^5 with fixed transition.

II. Flapping Kinematics

The two-dimensional motion of an oscillating airfoil is usually combined of a plunging $z(t/T)$ motion and a pitching oscillation $\varphi(t/T)$ around the quarter-chord for one flapping period $0 \le t/T < 1$:

$$z(t/T) = \hat{z} \cdot \cos(2\pi t/T)$$

$$\varphi(t/T) = \hat{\varphi} \cdot \cos(2\pi t/T + \pi/2) + \varphi_0 \tag{1}$$

In this contribution, the aerodynamic effect of an additional, superimposed gliding motion $x(t/T)$

$$x(t/T) = \hat{x} \cdot \cos(2\pi t/T) \tag{2}$$

in the direction of the freestream velocity U_∞ is investigated (see Figs. 1a and 1b). As usual in aerodynamics, it is assumed that the coordinate system (x, z) moves with freestream velocity U_∞. Both plunging and gliding motions alter the AOA, which acts on the airfoil in its moving frame of reference (see Figs. 1c and 1d). Thus, the geometric AOA $\varphi(t/T)$, which is noticed by the observer in the inertial (x, z) coordinate system, is perceived as an effective angle of attack $\alpha_{\text{eff}}(t/T)$ from the airfoil in its periodically moving frame of reference. Because $\varphi(t)$, $\dot{z}(t)$, and $\dot{x}(t)$ are periodic functions, $\alpha_{\text{eff}}(t/T)$ will also be a periodic function. The amplitude of its first sinusoidal harmonic is called the amplitude of the effective AOA $\Delta\alpha_{\text{eff}}$. Usually, the frequency of the flapping motion $f = 1/T$ is made nondimensional using the equation

$$k = \frac{\pi f c}{U_\infty} \tag{3}$$

where k represents the reduced frequency, a measure for the aerodynamic unsteadiness of the flow. The inverse of k describes how far the undisturbed air travels in airfoil chord lengths c during one flapping cycle. In other words, it is the ratio of the distance that a flapping flyer would make in a forward direction during one flapping cycle to the airfoil chord length c. For seagull flight conditions, k has values around 0.2 [5]. Further, the pitch-plunge amplitude ratio λ is introduced:

$$\lambda = \frac{\hat{\varphi}}{\arctan(2k\frac{\hat{z}}{c})} \tag{4}$$

The inviscid theory of Theodorsen [6] and Garrick [7] states that the propulsive efficiency for different combinations of pitch and plunge motions remain approximately constant if the parameter λ is kept constant. Windte and Radespiel [8] reported that a choice of $\lambda = 0.8$ guarantees high propulsive efficiencies when the reduced frequency is $k = 0.25$. The motion-parameter cases of Table 1 were investigated in this contribution.

III. Propulsive Efficiency

The flapping motion creates unsteady aerodynamic forces $F_x(t)$ and $F_z(t)$, which are measured in the (x, z) coordinate system and act at the quarter-chord (see Fig. 1d). $F_x(t)$ has the same direction as the freestream velocity U_∞. It would seem that thrust seems to be generated when $F_x < 0$. However, this definition is not entirely correct, because if $F_x = 0$, then an amount of thrust is already produced that compensates for the static drag of the airfoil. In consequence, compared to conventional aircraft, drag and thrust of a flapping airfoil have to be separated artificially because these forces are generated by an "all-in-one" integral system. To compute the thrust coefficient c_t, Windte and Radespiel [8] subtracted the static drag coefficient $c_{x,\text{stat}}$ of the airfoil at the mean angle of attack φ_0 from the force coefficient $c_x(t/T)$:

$$c_t = -[c_x - c_{x,\text{stat}}(\varphi_0)] \tag{5}$$

where c_x is a force coefficient relating to the force F_x, which is made nondimensional, $c_x = \frac{F_x}{\frac{\rho_\infty}{2} U_\infty^2 \cdot c \cdot \text{span}}$. Herein, ρ_∞ represents the fluid density at free-stream conditions. For the investigated birdlike airfoil SG04, $c_{x,\text{stat}} = 0.015$ results from the airfoil polar published in [4]. The thrust force acts upstream, i.e., c_t is positive when thrust is produced. According to early work of Garrick [7], the propulsive efficiency η_p is computed by

$$\eta_p = \frac{\int_0^T c_t U_\infty \, \mathrm{d}t}{-\int_0^T (c_x \dot{x} + c_z \dot{z} + c_m \dot{\varphi} c) \, \mathrm{d}t} \tag{6}$$

The numerator of this equation describes the work of thrust. The denominator contains the input work to sustain the flapping motion. The plunging oscillation $\dot{z}$ works against the lift force (coefficient) c_z, thus the negative sign in the denominator, the gliding oscillation $\dot{x}$

Received 17 November 2011; revision received 17 February 2012; accepted for publication 21 February 2012.

*Research Associate, Institute of Fluid Mechanics, Bienroder Weg 3; s.bansmer@tu-braunschweig.de.

†Head of the Institute, Institute of Fluid Mechanics, Bienroder Weg 3. Senior Member AIAA.

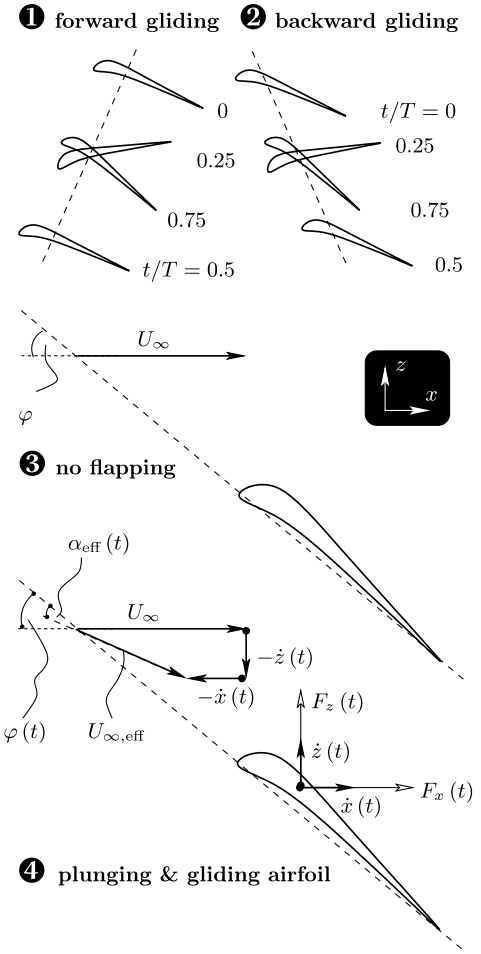

Fig. 1 Flapping kinematics in the inertial, aerodynamic coordinate system (x, z), which moves with freestream velocity U_∞: (a) Flapping motion with superimposed forward gliding motion during the downstroke ($\hat{x}/\hat{z} > 0$). Top dead center of the motion at $t/T = 0$. (b) Flapping motion with superimposed backward gliding motion during the downstroke ($\hat{x}/\hat{z} < 0$). (c) Geometric angle of attack (AOA) φ at steady conditions. (d) The change from geometric $\varphi(t)$ to effective angle of attack $\alpha_{\text{eff}}(t)$ due to the plunging $\dot{z}(t)$ and gliding $\dot{x}(t)$ motions. Further, the flapping motion creates aerodynamic loads $F_x(t)$ and $F_z(t)$ that are varying during one flapping cycle. Both forces are measured in the inertial coordinate system (x, z).

works against the c_x force (coefficient), and the pitch oscillation $\dot{\varphi}$ works against the aerodynamic pitch moment (coefficient) c_m.

IV. Numerical Scheme

To compute the aerodynamic problem of flapping airfoils, the URANS equations are solved using the FLOWer code [9], which requires block-structured meshes. The discretization scheme is a finite-volume approach. A second-order accurate central-difference scheme with scalar dissipation was applied to evaluate convective fluxes. Implicit residual smoothing, local time stepping, preconditioning, and multigrid operations were performed to accelerate the computation. A second-order accurate implicit dual time-stepping scheme was used for the time-accurate computations. The two-layer k-ε model of Menter [10] was chosen for the turbulence modeling. The model equations are computed on a single grid. A transition prediction based on the e^N method is available; however, the transition laminar-turbulent was fixed on the upper side of the airfoil at $x_t^*/c = 0.1$ and on the lower side at $x_t^*/c = 0$. This transition fix was necessary because the e^N method is only a good choice for flow governed by convective instabilities and moderate stall. In the investigated parameter space, deep stall was present. A grid convergence study presented in [4] demonstrated that a grid resolution of 544×112 cells is appropriate for the simulations. The far-field distance is about twenty times the chord length. Furthermore, the numerical scheme was validated with stereoscopic particle image velocimetry measurements for the case of the flapping SG04 airfoil with predominant attached-flow conditions including laminar separation bubbles [4].

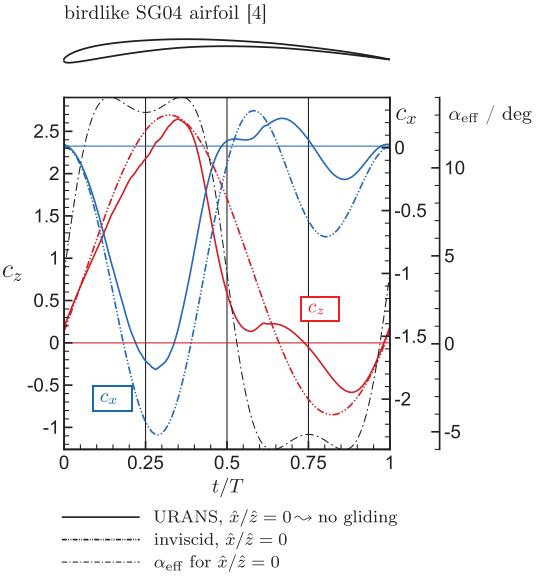

Fig. 2 History of lift and drag coefficient for one flapping period, comparison between inviscid and URANS solution, motion case VI, motion without gliding, $\lambda = 0.8$, $\Delta\alpha_{\text{eff}} = 9$ deg, $c_{x,\text{stat}} = 0.015$ (from airfoil polar published in [4]).

V. Results

A. Flapping Flight without Gliding Motion

The history of lift (c_z) and c_x-force coefficient over one flapping period is plotted in Fig. 2 for the motion-parameter case VI. The value $t/T = 0$ corresponds to the top dead center of the motion, thus the downstroke takes place during $0 \le t/T < 0.5$. The URANS solution, plotted as a solid line, is compared to the result of the inviscid theory of Theodorsen and Garrick [6,7] and is drawn as a

Table 1 Flapping motion parameters for the URANS computations

Motion case no.		I	II	III	IV	V	VI
Reynolds number	Re	10^5					
Reduced frequency	k	0.2					
Chord length	c	0.2 m					
Lambda [Eq. (4)]	λ	0.8					
Phase difference between pitch-plunge	$\Delta\Psi$	90 deg					
Mean AOA	φ_0	4 deg					
Amplitude effective AOA	$\Delta\alpha_{\text{eff}}$	4 deg	5 deg	6 deg	7 deg	8 deg	9 deg
Amplitude geometrical AOA	$\hat{\varphi} = \frac{\lambda \cdot \Delta\alpha_{\text{eff}}}{1-\lambda}$	16 deg	20 deg	24 deg	28 deg	32 deg	36 deg
Plunging amplitude	$\frac{\hat{z}}{c} = \frac{\tan(\frac{\hat{\varphi}}{2})}{2k}$	0.91	1.17	1.44	1.75	2.10	2.50

dash-dot-dot line. The lift coefficient (red plot) peaks during the downstroke due to the high effective AOA (α_{eff} about 14 deg) in this phase. Furthermore, most thrust is produced [$c_t > 0$, i.e., $c_x < c_{x,\text{stat}}$, see Eq. (5)] during the downstroke (blue plot). This can be explained by the Knoller–Betz effect; the effective AOA is high during the downstroke, although the geometric AOA is less than 0 deg, resulting in a component of the lift force, which is directed upstream and acts as thrust. The result also indicates the viscous effect of the boundary layer and eddy formation in the flow field. Particularly during the downstroke, less lift and less thrust is generated than predicted by the inviscid theory.

Based on the history plots, integral quantities like mean lift $\bar{c}_z$ and mean thrust $\bar{c}_t$ can be derived:

$$\bar{c}_z = \frac{1}{T}\int_0^T c_z \, \mathrm{d}t$$

$$\bar{c}_t = \frac{1}{T}\int_0^T c_t \, \mathrm{d}t$$

Figure 3 depicts the propulsive efficiency η_p and the mean lift coefficient $\bar{c}_z$ versus the mean thrust coefficient $\bar{c}_t$ for the motion cases I–VI without forward gliding ($x = 0$) at constant λ and increasing amplitude of the effective AOA (solid line with square dots). When the amplitude of the effective AOA $\Delta\alpha_{\text{eff}}$ is increased, the mean thrust increases but the propulsive efficiency decreases from 87 to 70% in the investigated parameter space. The inviscid result (solid line with diamond points) predicts significantly higher efficiencies because the viscous effect of the boundary layer and dynamic-stall vortices that are created for large amplitudes of the effective AOA and is not covered by this theory.

The mean lift coefficient increases from 0.85 ($\Delta\alpha_{\text{eff}} = 4$ deg) to 0.87 ($\Delta\alpha_{\text{eff}} = 6$ deg), and decreases subsequently for increasing amplitudes of the effective AOA. This decrease can be explained by the onset of dynamic stall vortices [11] that develop from light stall towards a deep stall scenario.

The flow field for the motion case VI with dynamic stall is depicted in Fig. 4. For eight consecutive moments in time, the rotation $\omega = \text{rot}\,\vec{v}$ and streamlines in the frame of reference of the moving airfoil are plotted. The rotation is made nondimensional with a reference rotation $\omega_{\text{ref}} = \frac{1}{c}\sqrt{\frac{p_\infty}{\rho_\infty}} = 1437\frac{1}{s}$, which is computed with the chord length c of the airfoil and free-stream values of pressure p_∞ and density ρ_∞. During the downstroke, the effective AOA increases from 4 to 13 deg and causes an intense leading-edge stall-vortex on the upper side of the airfoil. In this process, the pressure changes propagate with the speed of sound much faster than the viscous response, and a very high lift coefficient of $c_z = 2.5$ can be achieved (see also Fig. 2). Under steady conditions, the airfoil would stall at $c_z = 1.3$, which corresponds to a static stall AOA of about 9 deg. The rapid change of the geometrical AOA close to the bottom dead center of the motion induces a counterrotating trailing-edge vortex. Because the effective AOA decreases to −5 deg during the following upstroke, the vortex system cannot be sustained and is shed into the wake. On the other hand, the small effective AOA of −5 deg induces at $t/T = 6/8$ for a short time a small leading-edge stall-vortex on the lower side of the airfoil.

B. Flapping Flight with Superimposed Gliding Motion

Now, the effect of gliding motions according to Eq. (2) is analyzed, which are superimposed on the motion cases I, III, and VI (see also the motion illustration in Figs. 1a and 1b). The dotted lines in the $\eta_p - \bar{c}_t$ plot in Fig. 3 demonstrate that a small superimposed forward gliding motion during the downstroke ($\hat{x}/\hat{z}$ about 1/8, see also Fig. 1a for a motion visualization) yields reasonable increase in both efficiency and thrust production. This behavior is observed for small and large amplitudes of effective AOA ($\Delta\alpha_{\text{eff}} = 4$, 6, and 9 deg, i.e., cases I, III, and VI). One disadvantage of the superimposed forward gliding motion during the downstroke is the reduction of the mean lift coefficient (see the dotted lines in the $\bar{c}_z - \bar{c}_t$ plot of Fig. 3). Hereby, penalties of about $\Delta\bar{c}_z = 0.1$ are noticed. However, a superimposed

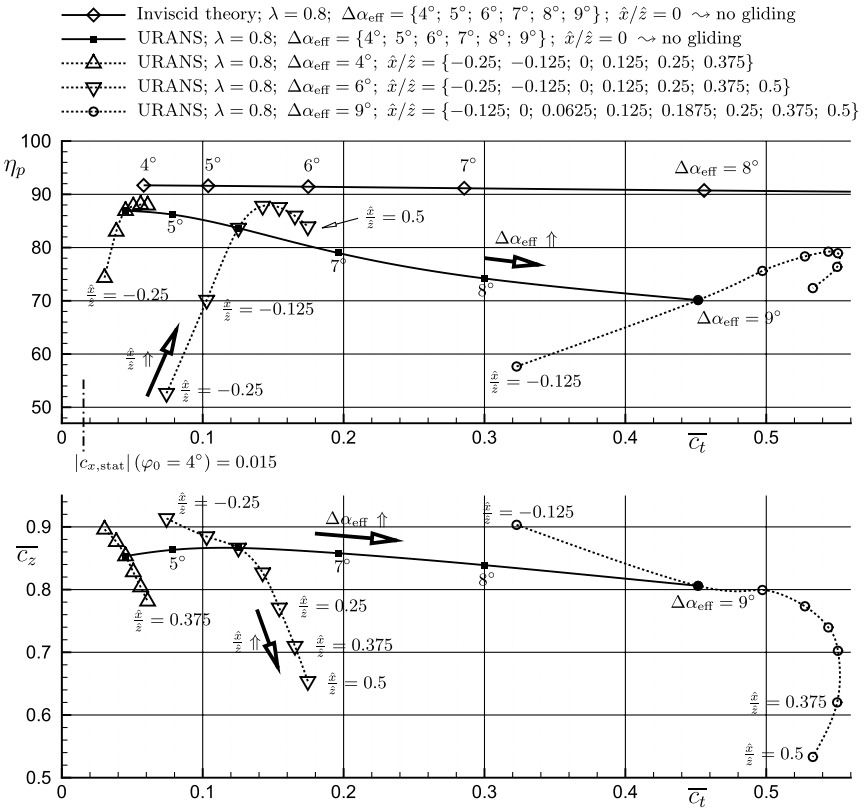

Fig. 3 Parametric study on the propulsive efficiency η_p (upper figure) and the mean lift coefficient $\bar{c}_z$ (lower figure) of the oscillating SG04 airfoil with $\lambda = 0.8$. Motion cases I–VI without superimposed gliding motion ($\hat{x}/\hat{z} = 0$) are drawn as solid lines. On cases I, III, and VI, gliding oscillations $x(t) = \hat{x} \cdot \cos(\omega t)$ were superimposed, drawn as dotted lines. $c_{x,\text{stat}} = 0.015$ from the airfoil polar published in [4].

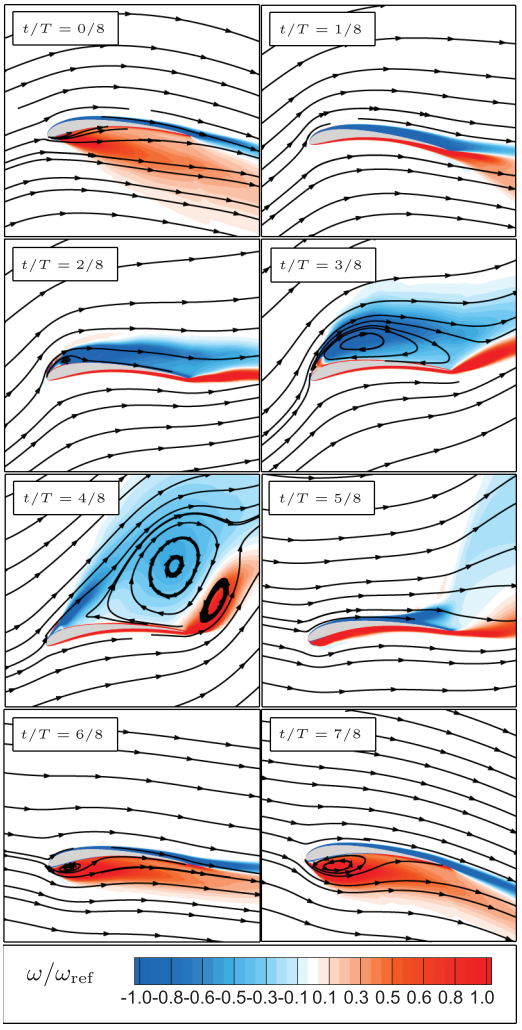

Fig. 4 Flow field for motion case VI ($\Delta\alpha_{\text{eff}} = 9$ deg) without gliding motion. Large areas of separated flow are present, $\omega_{\text{ref}} = \frac{1}{c}\sqrt{\frac{p_\infty}{\rho_\infty}} = 1437\frac{1}{s}$.

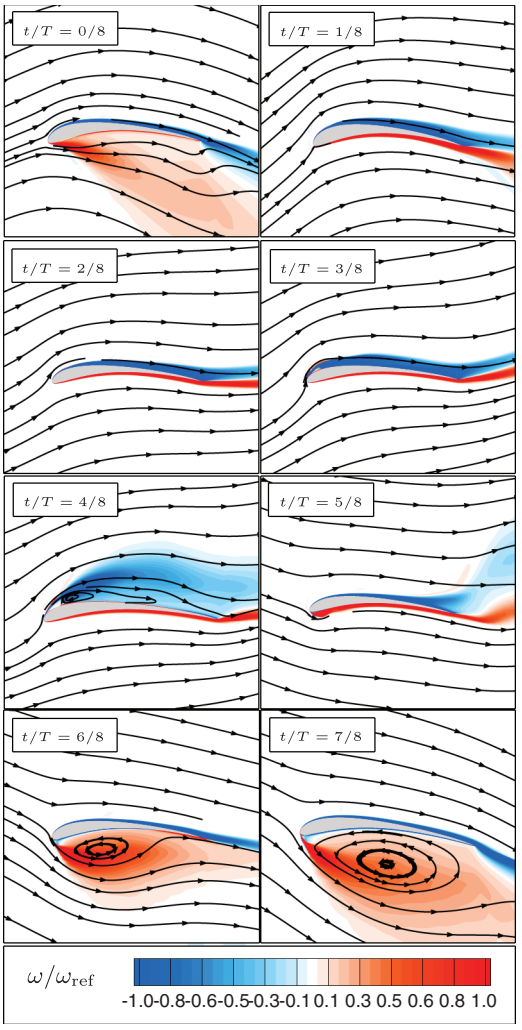

Fig. 6 Flow field for Case VI $\Delta\alpha_{\text{eff}} = 9$ deg with superimposed gliding motion ($\hat{x}/\hat{z} = 0.1875$), $\omega_{\text{ref}} = \frac{1}{c}\sqrt{\frac{p_\infty}{\rho_\infty}} = 1437\frac{1}{s}$.

backward gliding motion during the downstroke ($\hat{x}/\hat{z} < 0$, see also Fig. 1b for a motion visualization) shows the potential for lift increase. A comparison of motion case VI with and without a superimposed forward-gliding motion of $\hat{x}/\hat{z} = 0.1875$ can be found in Fig. 5, which shows the history of lift (c_z) and c_x-force coefficient over one flapping period for both cases.

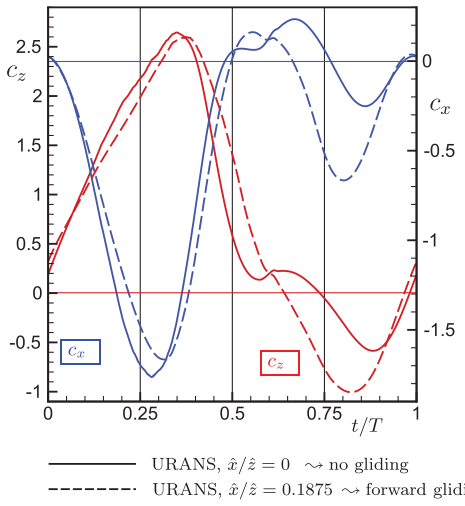

Fig. 5 History of lift and drag coefficient for one flapping period, comparison between pure pitch/plunge solution and superimposed gliding oscillation, $\lambda = 0.8$, $\Delta\alpha_{\text{eff}} = 9$ deg.

As illustrated by the streamlines in Fig. 6, the forward gliding motion during the downstroke reduces the effective AOA, resulting in a smaller region of separated flow on the upper side of the airfoil. Moreover, this yields higher lift coefficients for $0.35 \leq t/T < 0.55$. The effect of the gliding motion becomes more important during the upstroke for $0.6 \leq t/T < 0.9$. During this phase, a significant amount of extra thrust is generated. The backward gliding motion during the upstroke reduces the effective AOA significantly and a large separation vortex is formed on the lower side of the airfoil, which raises a negative lift. Because the geometrical AOA is large in this phase, the negative lift has a force component in upstream direction, acting as thrust. This is the Knoller–Betz effect of the upstroke motion.

VI. Conclusion

The aerodynamic effect of superimposed forward gliding oscillations parallel to the free stream velocity on a classical flapping motion (combined pitch/plunge motion) is investigated with unsteady Reynolds-averaged Navier–Stokes simulations and is compared with results of an inviscid theory. It is shown that superimposed forward gliding motions during the flapping downstroke, which are observed on flapping birds in nature, increase both propulsive efficiency and thrust. For cruise flight conditions at low thrust (motion case I), the efficiency increase is small; however, for long-range flight missions, even a marginal efficiency gain of 1% will be

noticeable. The demonstrated efficiency gain of up to 10% for maneuvering flight conditions with high thrust (motion case VI) suggests superimposed forward gliding motions as a new design paradigm for future micro air vehicle design. The study is performed for motion cases with low and high amplitudes of effective AOA. For high amplitudes of effective AOA, the phenomenon of dynamic stall is observed. In these cases, the prediction of lift, thrust and efficiency fails when using an inviscid theory.

Acknowledgments

As a part of the priority program SPP 1207, this project is funded by the German Research Foundation (DFG).

References

[1] Abate, G., and Shyy, W., "Introduction: Biologically Inspired Aerodynamics," *AIAA Journal*, Vol. 46, No. 9, 2008, pp. 2113–2114. doi:10.2514/1.35949

[2] Mueller, T. J. (ed.), *Fixed and Flapping Wing Aerodynamics for Micro Air Vehicle Applications*, Vol. 195, Progress in Astronautics and Aeronautics, AIAA, Reston, VA, 2001.

[3] Brown, R. H. J., "The Flight of Birds—The Flapping Cycle of the Pigeon," *Journal of Experimental Biology*, Vol. 25, No. 4, 1948, pp. 322–333.

[4] Bansmer, S., Radespiel, R., Unger, R., Haupt, M., and Horst, P., "Experimental and Numerical Fluid-Structure Analysis of Rigid and Flexible Flapping Airfoils," *AIAA Journal*, Vol. 48, No. 9, 2010, pp. 1959–1974. doi:10.2514/1.J050158

[5] Bansmer, S., and Radespiel, R., "Validation of Unsteady Reynolds-Averaged Navier–Stokes Simulations on Three-Dimensional Flapping Wings," *AIAA Journal*, Vol. 50, No. 1, 2012, pp. 190–202. doi:10.2514/1.J051226

[6] Theodorsen, T., "General Theory of Aerodynamic Instability and the Mechanism of Flutter," NACA TM 496, 1935.

[7] Garrick, I., "Propulsion of a Flapping and Oscillation Airfoil," NACA Rept. No. 567, 1936.

[8] Windte, J., and Radespiel, R., "Propulsive Efficiency of a Moving Airfoil at Transitional Low Reynolds Numbers," *AIAA Journal*, Vol. 46, No. 9, 2008, pp. 2165–2177. doi:10.2514/1.30569

[9] Kroll, N., Rossow, C. C., Schwamborn, D., Becker, K., and Heller, G., "MEGAFLOW: A Numerical Flow Simulation Tool for Transport Aircraft Design," *International Council of the Aeronautical Sciences, ICAS*, Paper No. 1105, 2002.

[10] Menter, F., "Two-Equation Eddy-Viscosity Transport Turbulence Model for Engineering Applications," *AIAA Journal*, Vol. 32, No. 8, 1994, pp. 1598–1605. doi:10.2514/3.12149

[11] McCroskey, W., "The Phenomenon of Dynamic Stall," NASA TM-81264, 1981.

R. Gordnier
Associate Editor